AD-A091 744 MASSACHUSETTS UNIV AMHERST ASTRONOMY RESEARCH FACILITY F/G 4/1
INFRARED EMISSION SPECTROSCOPY OF LOW PRESSURE GASEOUS DISCHARG--ETC(U)
MAY 80 H SAKAI F19628-76-C-0087
UNCLASSIFIED UMASS-ARF-80-309 AFGL-TR-80-0157 NL

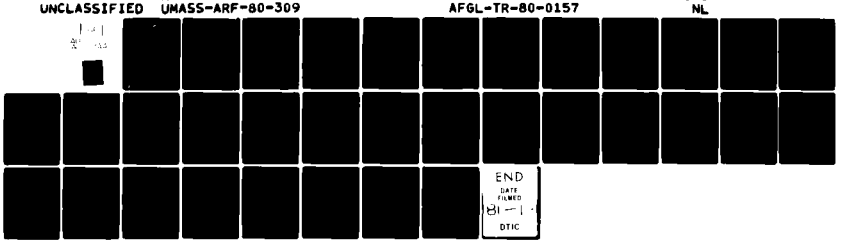

END
DATE FILMED
8I-1
DTIC

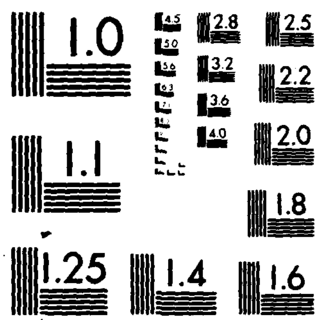

OK Level III

12
B.S

AFGL-TR-80-0157

AD A091744

INFRARED EMISSION SPECTROSCOPY OF LOW PRESSURE GASEOUS DISCHARGES, III

Hajime Sakai

Astronomy Research Facility
University of Massachusetts
Amherst MA 01003

May 1980

Scientific Report No. 3

AIR FORCE GEOPHYSICS LABORATORY
AIR FORCE SYSTEMS COMMAND
UNITED STATES AIR FORCE
HANSCOM AFB, MASSACHUSETTS 01731

UNCLASSIFIED

SECURITY CLASSIFICATION OF THIS PAGE (When Data Entered)

12 33

18 19 REPORT DOCUMENTATION PAGE

READ INSTRUCTIONS BEFORE COMPLETING FORM

REPORT NUMBER: AFGL-TR-80-0157

2. GOVT ACCESSION NO.: AD-A091744

3. RECIPIENT'S CATALOG NUMBER: 9

4. TITLE (and Subtitle): INFRARED EMISSION SPECTROSCOPY OF LOW PRESSURE GASEOUS DISCHARGES. III.

A078796

5. TYPE OF REPORT & PERIOD COVERED: Interim rept., Scientific Report No. 3

6. PERFORMING ORG. REPORT NUMBER: UMASS-ARF-80-309, SCIENTIFIC-3

14

7. AUTHOR(s): Hajime/Sakai

15

8. CONTRACT OR GRANT NUMBER(s): F19628-76-C-0087

9. PERFORMING ORGANIZATION NAME AND ADDRESS: Astronomy Research Facility, University of Massachusetts, Amherst MA 01003

16

10. PROGRAM ELEMENT, PROJECT, TASK AREA & WORK UNIT NUMBERS: 61102F, 2310G409

17 G4

11. CONTROLLING OFFICE NAME AND ADDRESS: Air Force Geophysics Laboratory, Hanscom AFB, Massachusetts 01731, Monitor/Alastair Fairbairn/OPR

11

12. REPORT DATE: May 1980

13. NUMBER OF PAGES: 32

14. MONITORING AGENCY NAME & ADDRESS (if different from Controlling Office)

15. SECURITY CLASS. (of this report): Unclassified

15a. DECLASSIFICATION/DOWNGRADING SCHEDULE

16. DISTRIBUTION STATEMENT (of this Report)

Approved for public release; distribution unlimited.

17. DISTRIBUTION STATEMENT (of the abstract entered in Block 20, if different from Report)

18. SUPPLEMENTARY NOTES

19. KEY WORDS (Continue on reverse side if necessary and identify by block number)

Emission spectra
Fourier spectroscopy
Gaseous discharge
Infrared

20. ABSTRACT (Continue on reverse side if necessary and identify by block number)

Our study conducted on the infrared NH band is described in this report. The emission was observed both in decomposition and in recombination processes.

The spectroscopic constants of the NH ground state ($X^3\Sigma^-$) are determined using the data obtained with a resolution of 0.2 cm^{-1}.

DD FORM 1 JAN 73 1473 EDITION OF 1 NOV 65 IS OBSOLETE

UNCLASSIFIED

SECURITY CLASSIFICATION OF THIS PAGE (When Data Entered)

406989

I. Infrared Emission of NH Free Radical

The present work follows our two previous scientific reports[1,2] for Contract No. F19628-76-C-0087. This report deals with our analysis effort for the observed NH infrared band in 2500 ∿ 3300 cm^{-1}. The free radical NH is known to form in decomposition of NH_3. The uv band of NH is one of the bright uv features in the decomposition. The band identified as the transition $A^3\pi_i - X^3\Sigma^-$ was analyzed by Dixon[3] and more recently by Malicet et al.[4] In contrast to the uv emission, the infrared band has never been reported in the literature. In fact, the observation of the infrared NH band was a big surprise to us in two aspects: (1) the NH is a very bright emitter; and (2) it is formed in the recombination process as well as in the decomposition process.

This report is divided into three sections: (1) the experimental description involving the detection of the NH infrared band, presented at the SPIE meeting held at San Diego, August 1979; (2) the spectral analysis of the infrared NH band, presented at the Symposium of Molecular Spectroscopy held at the Ohio State University, June 1979; and (3) a description of the N_2 excited states and the formation mechanism of NH.

The NH radical could play a role in perturbations of the upper atmosphere. Its chemical reaction rate to destroy NO is fast.[5] In our discharge condition, the suppression of the NO fundamental is strongly correlated with the increased emission of the NH fundamental.

Our study on the NH infrared emission was carried out by three persons. Peter Hansen did the interferogram measurements, and Mark Esplin did the spectral analysis. H. Sakai directed the entire effort and was in charge of writing this report.

References

1. P. Hansen, H. Sakai, and J. Strong, AFGL-TR-77-0251 (1977).
2. P. Hansen and H. Sakai, AFGL-TR-79-0150 (1979).
3. R.N. Dixon, Can. J. Phys. 37, 1171 (1959).
4. J. Malicet et al, J. Chem. Phys. Fr. 67, 25 (1970).
5. I. Hansen et al, Chem. Phys. Lett. 42, 370 (1976).
   J. Mulvihill et al, Chem. Phys. Lett. 35, 327 (1975).

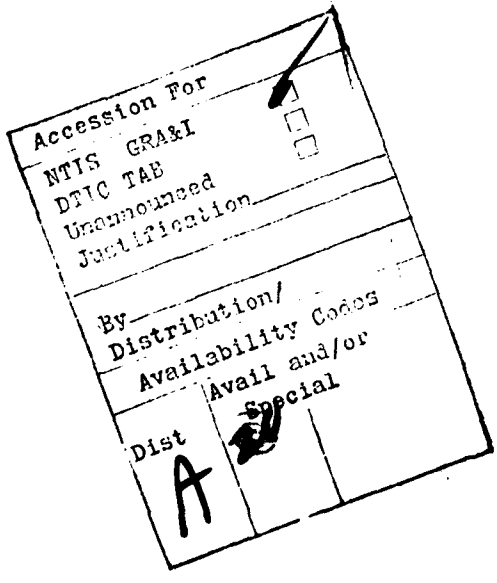

A Reprint from the

PROCEEDINGS

OF THE SOCIETY OF PHOTO-OPTICAL INSTRUMENTATION ENGINEERS

Volume 191

Multiplex and/or High-Throughput Spectroscopy

August 27-28, 1979
San Diego, California

Observation of NH infrared emission using Fourier spectroscopy

Peter Hansen, Hajime Sakai, Mark Esplin
Astronomy Research Facility, University of Massachusetts
Amherst, Massachusetts 01003

Observation of NH infrared emission using Fourier spectroscopy

Peter Hansen, Hajime Sakai and Mark Esplin
Astronomy Research Facility, University of Massachusetts
Amherst, Massachusetts 01003

Abstract

The technique of Fourier spectroscopy is instrumental in achieving a high sensitivity for the spectrometry of detecting weak infrared emission sources. In our survey study conducted on the infrared emission of the atmospheric species, this fact is fully appreciated; both the multiplex advantage and the interferometric gain on collecting the infrared photons, together with our emission source of a 36-meter-long electric discharge column, are essential to detect various atmospheric bands and lines, some well known and some little known. Lately, we succeeded to observe the infrared vibration fundamental band of NH which was previously undetected.

Introduction

In recent years, many studies have been focused on the problems associated with the infrared radiation observable in the upper atmosphere. Identification of the spectral features in the observed radiation is a key to improve our understanding of the physics and chemistry problems relating to the upper atmosphere. The recent rocket data obtained by the Air Force Geophysics Laboratory[1] revealed an intense band structure in the spectral region between 2800 and 3500 cm^{-1}. The band is clearly distinguishable from the 4.3 micron CO_2 band and it spreads in a range much broader than what is generally considered of the OH vibrational fundamental ($\Delta v = 1$). We at UMass have been engaged in a laboratory experimental program which studies the physical chemistry of the upper-atmospheric infrared radiation through the spectrometric technique.[2] In so doing, an electric discharge column of enormous size is formed at low pressure, and the resulting infrared emission is studied by using the technique of Fourier spectroscopy. Recently we detected a spectral feature which is identifiable with the one seen between the 4.3 micron CO_2 band and the OH vibrational fundamental in the AFGL rocket data. Consequently, we succeeded to identify the feature as the NH vibrational fundamental. The results obtained from the spectral analysis of this band have already been reported by us at another meeting.[3] In this paper we will present the technical side of our experimental effort.

Our interest is focused on the region in the upper atmosphere above 60 km, where the pressure remains below 1 torr. Our study is concentrated on the infrared emission generated by electronic excitation at a level of 20 ~ 30 eV at such a low atmospheric pressure. Our basic experimental approach to the study is twofold: (1) by forming a long electric discharge column to produce the infrared photons of various atmospheric species in a large number; and (2) by using Fourier multiplex spectrometry to optimize the efficiency of collecting the generated infrared photons. By combining these two features, we were able to enhance the detection sensitivity to such a level that only 15 minutes observation time is required to cover the entire InSb spectral range (1800 - 7800 cm^{-1}) with a resolution of 1 cm^{-1}.

Experimental setup

A central feature of our experimental setup is a 30-meter long, 1-meter diameter cylinder used as a container of the discharge source, which is formed between a 12-meter long central electrode and the external wall as shown in Fig. 1. An a.c. 60 Hz voltage of up to 1000 V is applied between the electrodes, activating the discharge. The interferometer accepts the infrared radiation through a KBr lens placed at the exit port of the discharge source. The interferogram signal is detected by an InSb detector housed in a liquid nitrogen dewar. The path difference is monitored by the interference fringe signal of the HeNe cw laser line 6328 Å (air wavelength). The detector output is properly ac-amplified, synchronously demodulated, integrated, and finally converted to a digital signal by an analog-to-digital converter, which is triggered by the zero-crossing position of the laser interference fringe reference signal. The digitized interferogram signal is then recorded on a mass storage device (a floppy disk) under the control of an LSI-11 minicomputer. After completion of the interferogram measurement, the interferogram data is post-processed using our central-site large-scale computer, CDC Cyber system, for the Fourier transformation, etc. Our data acquisition scheme is shown schematically in Fig. 2.

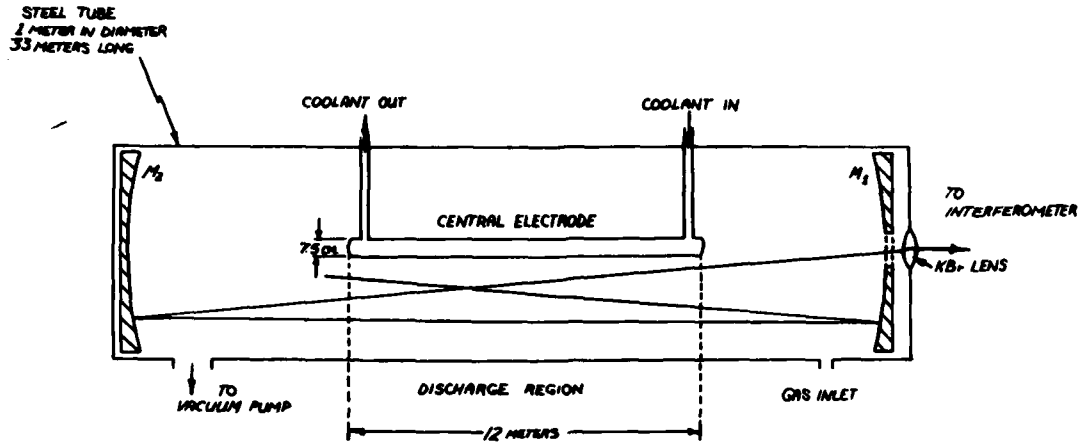

Fig. 1. Schematic representation of the discharge column (not to scale). Mirrors M_1 and M_2 are focused on each other, resulting in three passes through the discharge column.

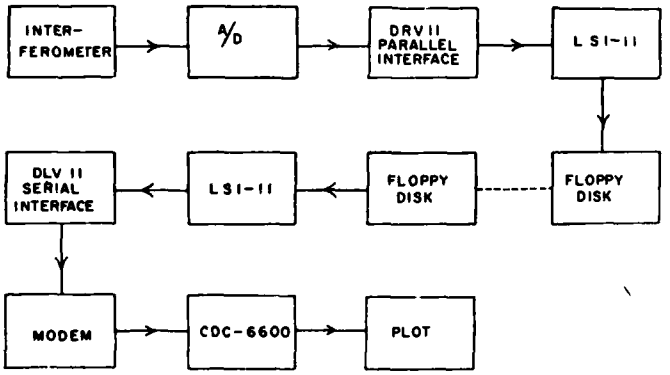

Fig. 2. Data collection and processing scheme.

There are two components which crucially affect our experiment and which we will discuss in detail. One is the source arrangement, and the other is the interferogram data acquisition scheme.

Source

The optical cell which is used to house our glow discharge source is generally known as the "Pfund" cell. The discharge column formed between the electrodes is seen thrice along the optical path, thus forming an equivalent 36-meter long discharge column. The discharge region extends only 1/3 of the entire cell length, leaving 2/3 of the cell a discharge-free space. This apparent disadvantage created by the discharge-free region is a blessing in disguise from the experimental point of view, since it prevents the mirror contamination caused by the electron bombardment.

An important parameter which controls our glow discharge is the excitation energy released to the atoms and the molecules. A rough estimate of the excitation energy can be obtained in the following way. The electric field in the cell is given as a function of a distance r (measured from the center) by

$$E = \frac{V}{r(\ln\frac{b}{a})}, \qquad (1)$$

where V is the electric potential applied between the electrode of radius a and the wall of radius b. The electrons pick up their energy under the applied electric field and lose

it when they collide with a molecule or atom. The loss of energy occurred at the collision turns into the energy for exciting the collision partners, for our case either molecule or atom. This energy loss suffered at the collision is usually resupplied between collisions. The mean free path <x> of these electrons, i.e., the mean distance between the successive collisions, is generally characterized by

$$\langle x \rangle = \frac{1}{n\sigma} \tag{2}$$

where n is the number density of the colliding molecules and σ a quantity called the collision cross-section. If an electron moves parallel to the field, it gains its energy by <x>eE, which is calculated by

$$E = e\langle x \rangle E = \frac{eVp_o}{r(\ln\frac{b}{a})N_o p}. \tag{3}$$

It is seen that the excitation is the highest in the vicinity of the electrode and that it reduces toward the outer wall. For a typical example, we can assume $\sigma \tilde{\sim} 10^{-16}$ cm^2, V = 1000, and $n = N_o p/p_o = 7.071 \times 10^{15}$ for p = 0.2 torr. The field at r = 30 cm is about 13 V/cm, while the mean free path is about 1.4 cm. The excitation at r = 30 cm would reach 18 eV = 145000 cm^{-1}. In reality, the electrons do not necessarily move parallel to the line of force, and the cross-section σ is dependent on the electron energy. Nonetheless, the value estimated above for the excitation energy agreed well with the experimental data obtained. In the glow discharge spectra of oxygen, for example, many infrared atomic oxygen lines are observed, which are produced in quantum transition between two highly excited atomic levels. By identifying the levels involved for the observed infrared atomic OI lines, it was found that the excitation energy in our glow discharge generally reaches a level of 20 eV. Even though some excitations may exceed this value by a substantial degree, it is safe to assume that a majority of the infrared photons observable in our experiment are indeed generated in the processes which require an excitation energy of about 20 eV or less.

One thing noticeable is that the excitation is very sensitive to the gas pressure. Once the gas pressure is above 0.5 torr, the glow discharge which is indicative of transitions between the electronic states is confined to the vicinity of the electrodes, leaving a dark space elsewhere. For heteronuclear molecules, the infrared emission does not necessitate the electronic transition. An absence of the visible glow discharge does not eliminate a possible infrared emission. However, for homonuclear molecules, the visible glow discharge which usually indicates a presence of the electronic transitions to the ground state is necessary to produce infrared transitions.

The voltage applied to produce a glow discharge is 60 Hz a.c. It is obtained from the ordinary 60 Hz power, through a step-up transformer. D.C. voltages did not produce stable discharges. The central electrode is usually water-cooled.

Data acquisition scheme

Two factors that require special attention when implementing infrared emission spectrometry are of particular concern to the quality of the spectral recovery achieved when using multiplex spectrometry. The first is an inherent intensity instability of the electric glow discharge source. The second is the temporal behavior of the excitation-relaxation processes of the various species. The physical condition leading to the glow discharge emission must be carefully adjusted for the maximum intensity stability. The d.c. discharge, as mentioned above, failed to produce the intensity stability required. The a.c. discharge was found to be much more stable, as it suppressed the formation of arcs. However, the a.c. discharge creates an excitation-relaxation sequence synchronized with the voltage cycle. Within each excitation-relaxation cycle, every spectral component produced in the discharge follows its own sequence pattern as a function of time, and it is expected to repeat this in every cycle. The data acquisition scheme must be implemented with this temporal aspect of the a.c. source in mind.

The electronics used in the conventional signal acquisition scheme, a lock-in amplifier, accomplishes the integration of a demodulated signal by an RC filter network which acts on the temporal flow. In consequence, it fails on two accounts. First, it produces no correction to non-uniformities of the interferometer drive.[4] Distortion in the obtained spectrum may become pronounced whenever one tries to push the interferogram measurement over a threshold path difference set by the drive non-uniformity. Secondly, it fails to correct a phase mismatch between the lock-in amplifier demodulation and the excitation-relaxation sequence of various spectral components.[5] The effect becomes pronouncedly evident in the infrared where the excitation-relaxation cycles vary considerably among the observable species because of a large difference in their radiative lifetimes.

At the time of writing this paper, we have not completed the electronics scheme which accommodates the time-resolved multiplex operation. Upon its completion, we plan to take the data with a time-resolved capability. Until now, we have taken all the data with the conventional lock-in amplifier scheme.

The interferogram data processing and the spectral data recovery are all performed using our central site CDC Cyber system. We hope to improve the present 300 BAUD data-linkage by installing a 1200 BAUD modem in the near future. For the processing of the 65,536-point interferogram data, which produces a spectral resolution of 0.12 cm^{-1} over the range of 0 to 7899 cm^{-1}, we believe that our off-line processing scheme is a workable and practical solution. In a case such as ours, where the emission spectra must be examined over a broad spectral range, the advantage offered by a large-data-point Fourier transform processing scheme using a large scale computer is well appreciated. With a fast CRT display scope directly connected to the main frame, we are able to inspect the data over a wide spectral range very efficiently.

Observation of NH infrared emission

The NH molecule is a free radical which reacts to the NO molecule with a fast reaction rate. It has been generally considered that the decomposition process, $NH_3 \rightarrow NH$, is the only feasible generation mechanism. The recombination process was excluded as ineffective for formation of NH.

The spectrum shown in Fig. 3 was obtained by the electric discharge in 0.1 torr of air, which corresponds to an altitude of 60 km in the atmosphere. The spectral feature

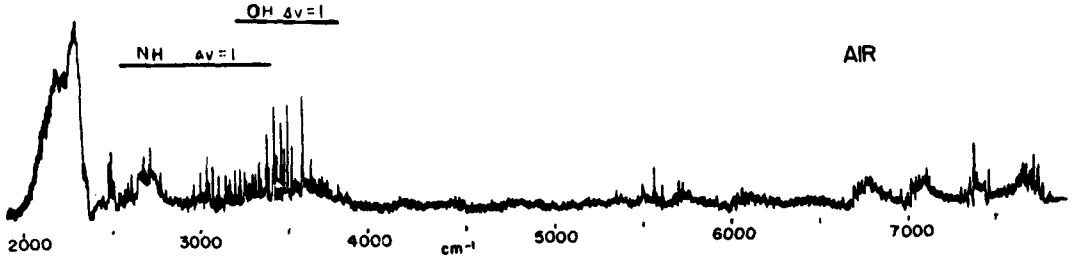

Fig. 3. Infrared emission spectrum produced by an electric discharge in air. Besides the indicated NH and OH emission, NO, CO, CO_2, N_2, OI and NI are also observed.

seen between 2700 cm^{-1} and 3500 cm^{-1} varied its intensity considerably from time to time. The higher cm^{-1} end of this feature was known to us already as the OH vibrational fundamental, $\Delta v = 1$. With the knowledge that the OH is formed as a derivative in the presence of H_2O, we reasoned that a parameter responsible for this phenomenon is the moisture content of the air used in the discharge source. Being afraid of an irreparable contamination to the electrodes caused by excessive H_2O, we substituted hydrogen, expecting the same effect. The spectrum shown in Fig. 4 was obtained by the discharge of

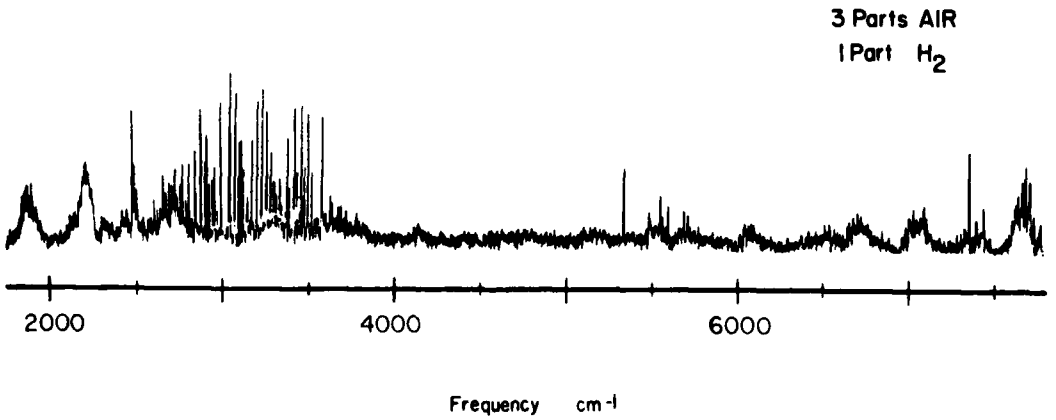

Fig. 4. The spectrum of an air/H_2 discharge. The addition of hydrogen to the air quenches CO_2 ($\Delta v_3 = 1$) emission. NH and OH become the dominant emitters, along with atomic hydrogen ($n = 5 \rightarrow 4$, $4 \rightarrow 3$).

air mixed with the hydrogen. We found, as expected, that the feature between 2700 cm^{-1} and 3500 cm^{-1} was indeed enhanced. As a matter of fact, it became the brightest emitter in the infrared range covered.

The problem of identifying the band was solved first by the spectral analysis. The molecular constants determined from the spectral analysis indicated that the band undoubtedly belongs to the NH vibrational fundamental. Later we confirmed this in spectra obtained by decomposing NH_3 in the discharge. Fig. 5 is the spectrum obtained by the decomposition process taken with a resolution of 1 cm^{-1}. Fig. 6 shows the well isolated NH fundamental with a spectral resolution of $\Delta\nu$ = 0.1 cm^{-1}.

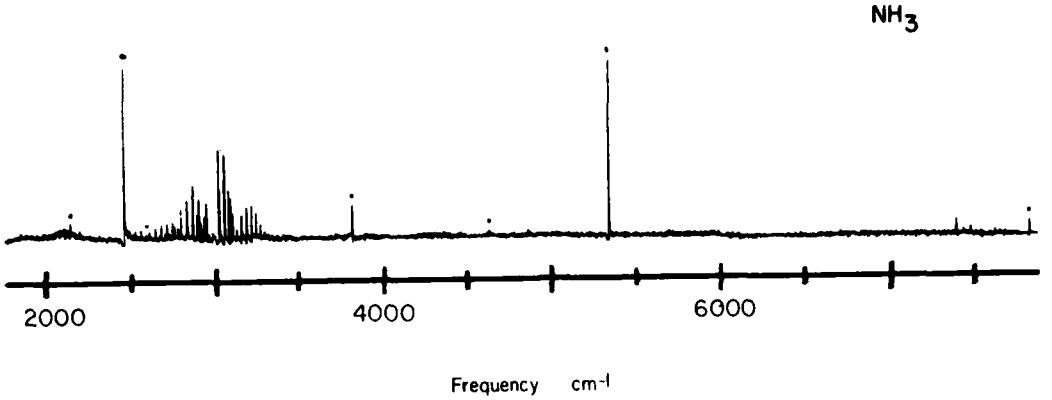

Fig. 5. Emission spectrum produced by an electric discharge in NH_3. The decomposition products NH and atomic hydrogen (dotted lines) are the observed emitting species. The NH fundamental is well isolated here.

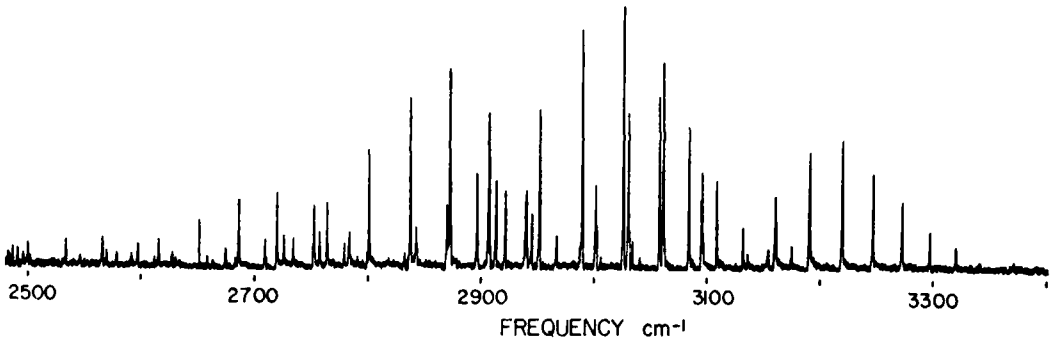

Fig. 6. The NH fundamental observed at higher resolution ($\Delta\nu$ = 0.1 cm^{-1}) in an NH_3 discharge.

Now that the NH is undoubtedly formed by recombination, the nature of the recombination process that is responsible for our observed NH spectra must be investigated. Having observed only atomic hydrogen lines in various spectroscopic data taken with the hydrogen-mixed gases, we concluded that very few hydrogen molecules are present in the discharge. The reaction in question is conceivably with the atomic hydrogen. If the NH were formed by the process

$$N_2 + H \rightarrow NH,$$

a time-resolved characteristic of the NH band should differ considerably from that of the N_2 bands or that of the HI emission. The time-resolved technique which we already developed[5] should produce some data giving a crucial solution to the problem stated above.

Conclusion

We have proved that the Fourier multiplex technique applied to the infrared emission spectrometry is indeed powerful. Its high spectrometric efficiency and wide spectral coverage are both essential to the study. The technique will produce a further impact to the study, as it will be extended to add one more multiplexing degree to it in terms of the time-resolved capability.

Acknowledgment

This work is supported by AFGL Contract No. F19628-76-C-0087.

References

1. R. Nadile *et al*, "SPIRE Program," paper presented at Topical Meeting on Atmospheric Spectroscopy, Keystone CO (1978).
2. P. Hansen and H. Sakai, "Infrared Emission Spectroscopy of Low Pressure Gaseous Discharge II," AFGL-TR-79-(in press), (1979).
3. M. Esplin, P. Hansen, and H. Sakai, paper presented at 34th Symposium on Molecular Spectroscopy, Ohio State University (1979).
4. H. Sakai and R. Murphy, J. Opt. Soc. Am. 60, 422 (1970).
5. R. Murphy, F. Cook, and H. Sakai, J. Opt. Soc. Am. 65, 600 (1975).

Question (Herbert Flicker, Los Alamos Scientific Laboratory): I gather that your Fourier transform spectrometer is of the step and modulate design. Did you lock into the 60 cycle excitation, and did you try locking in on a smaller time interval to insure quasi-static NH concentration during the measurement interval?

Answer: The lock-in amplifier is referenced to 120 Hz. The interferometer is of the continuous scanning type. We feel that narrowing the window is best done using digital techniques. We are presently implementing these.

II. The Infrared Spectrum of NH Vibrational Fundamental

The uv spectrum of the NH free radical, the transition between $A^3\pi$-$X^3\Sigma$, is well known for its emission feature in the NH_3 flame. The NH molecule is, in this case, formed by decomposition of NH_3. In our study conducted on the infrared emission of the atmospheric species, the vibrational fundamental transitions ($\Delta v = 1$) of the ground state $X^3\Sigma^-$ were found as one of the bright features in the mid-infrared region.[1] Our experimental data indicate that the free radical can be produced by recombination as well as by decomposition. The rotational energy levels of the $^3\Sigma$ state, being perturbed by the coupling of the electronic spin angular momentum, splits into a triplet fine structure. Spectroscopically this splitting is classified as the Hund case (b).[2] The electronic spin of unity adds to the rotational angular momentum, forming the total angular momentum J = N+1, J = N and J = N-1.

The rotational level of the $^3\Sigma$ system has been studied by many workers since the early days of quantum mechanics. Kramers derived the energy levels of those splitting in first approximation.[3] Hebb obtained an expression identical to the result derived by Kramers, although he interpreted his result quite differently.[4] The first approximation formula failed miserably when it was applied to the case of an oxygen molecule which has the electronic ground state wave function configuration $^3\Sigma^-$. Consequently, Schlapp recalculated the energy levels in a more exact expression for achieving an improved agreement.[5] Revisions to the Schlapp formula were later discussed in a series of papers by Miller and Townes,[6] Mizushima and Hill,[7] West and Mizushima,[8] and most recently by Steinback and Gordy.[9]

The rotational Hamiltonian for the $^3\Sigma$ state is given by

$$H_{rot} = B\hat{N}^2 + \frac{2}{3}\lambda\,(3S_\zeta^2 - \hat{S}^2) + \gamma\hat{N}\cdot\hat{S} \qquad (1)$$

where the first term represents the rotational kinetic energy, and the other two terms are the perturbation by the spin-spin and the spin-rotational coupling, respectively.[10] In this expression $\hat{N}$ is the angular momentum of the nuclear motion defined in the body-fixed axis, $\hat{S}$ is the electronic spin angular momentum, and S_ζ is the component along the molecular axis. B is the rotational constant, λ is the coupling constant for the spin-spin interaction, and γ is the coupling constant between $\hat{N}$ and $\hat{S}$.

The rotational energy is determined by solving the Hamiltonian, Eq. (1). Experimentally the rotational spectrum of the $^3\Sigma$ system retains a close resemblance with the $^1\Sigma$ system, which forms both the P and R branch corresponding to a change of N (=J for the $^1\Sigma$ system) by either -1 or +1. These rotational transitions are conventionally designated by either P(N) or R(N), where N refers to the rotational quantum number of the lower energy level.* A close inspection of the $^3\Sigma$ spectral lines reveals that they are split into three major lines grouped very closely and that other weaker lines are formed in a vicinity. Because the spectral pattern observable for the $^3\Sigma$ is very similar to the case for the $^1\Sigma$, the energy expression which is obtained by solving the Hamiltonian, Eq. (1), would take a convenient form for interpretation of the data

*For a complicated system, both transitions for ΔJ and ΔN are included in the designation as $(^{\Delta N}\Delta J_{N''N'})$. For an example, the transition between N'=3, J'=2, and N"=1, J"=2 is designated as $^SQ_{31}$, indicating $\Delta N=2$ between N'=3 and N"=1 and $\Delta J=0$.

if the rotational kinetic energy term $B\hat{N}^2$ is diagonal. (The angular momentum $\hat{N}$ is a component of the total angular momentum $\hat{J} = \hat{N} + \hat{S}$, which is a constant of motion. Thus N is not a good quantum number.) The rest in the Hamiltonian are treated as the perturbation term, even though the coupling constant λ may be larger than the rotational constant B as for the case of some molecules. The resulting expression would reduce to the familiar form of the $^1\Sigma$ case, E = BJ(J+1) or = BN(N+1), if those coupling constants, λ and γ, are very small. There exist many expressions derived for the $^3\Sigma$ system by many workers (References 3 through 10). Mizushima derived the most complete expression by extending the perturbation calculation to the second order:

$$\begin{aligned}\mathcal{E}_{rot}(J = n+1) = {} & B(n^2+3n+3) - D(n^4+6n^3+19n^2+30n+18) \\ & + H(n^6+9n^5+48n^4+153n^3+279n^2+270n+108) \\ & - \tfrac{1}{3}\lambda - \tfrac{1}{3}\lambda'(n^2+3n+6) - \tfrac{1}{2}\gamma - \tfrac{1}{2}\gamma'(7n^2+21n+18) \\ & - \sqrt{\Bigg[B(2n+3) - D(4n^3+18n^2+30n+18) \\ & \qquad + H(6n^5+45n^4+152n^3+279n^2+270n+108) - \\ & \qquad \frac{\lambda}{2n+3} - \frac{\lambda'(7n^2+21n+18)}{6n+9} - \tfrac{1}{2}\gamma(2n+3) - \\ & \qquad \tfrac{1}{2}\gamma'(2n^3+9n^2+21n+18)\Bigg]^2 + \\ & 4[\lambda + \lambda'(n^2+3n+3)]^2 \frac{(n+1)(n+2)}{(2n+3)^2}\end{aligned} \qquad (2)$$

$$\begin{aligned}\mathcal{E}_{rot}(J = N = n) = {} & Bn(n+1) - D[n(n+1)]^2 + H[n(n+1)]^3 + \tfrac{2}{3}\lambda + \tfrac{2}{3}\lambda' n(n+1) \\ & - \gamma - \gamma' n(n+1)\end{aligned} \qquad (3)$$

$$\begin{aligned}\mathcal{E}_{rot}(J = n-1) = {} & B(n^2 - n + 1) - D(n^4 - 2n^3 + 7n^2 - 6n + 2) \\ & + H(n^6 - 3n^5 + 18n^4 - 31n^3 + 33n^2 - 18n + 4) \\ & - \tfrac{1}{3}\lambda - \tfrac{1}{3}\lambda'(n^2 - n + 4) - \tfrac{3}{2}\gamma - \tfrac{1}{2}\gamma'(7n^2 - 7n + 4) \\ & + \sqrt{\Big[B(2n-1) - D(4n^3 - 6n^2 + 6n - 2) + \\ & \qquad H(6n^5 - 15n^4 + 32n^3 - 33n^2 + 18n - 4) - \\ & \qquad \frac{\lambda}{2n-1} - \frac{\lambda'(7n^2 - 7n + 4)}{6n - 3} - \tfrac{1}{2}\gamma(2n-1) - \\ & \qquad \tfrac{1}{2}\gamma'(2n^3 - 3n^2 + 9n - 4)\Big]^2 + \\ & \qquad 4\left[\lambda + \lambda'(n^2 - n + 1)\right]^2 \frac{n(n-1)}{(2n-1)^2}}\end{aligned} \tag{4}$$

where the coupling constants for both terms consist of two parts, a major term indicated by unprimed symbol, and a minor N-dependent term by primed symbol. If the rotational constant B is much larger than the coupling constants, λ or γ, and D = H = λ' = γ' = 0, the expression reduces to the Schlapp formula:

$$E(J=N+1) = BN(N+1) + (2N+3)B - \lambda - \sqrt{(2N+3)^2B^2 - 2\lambda B} + \gamma\,(N+1), \tag{5}$$

$$E(J=N) = BN(N+1) \tag{6}$$

and

$$E(J=N-1) = BN(N+1) - (2N-1)\,B - \lambda + \sqrt{(2N-1)^2B^2 + \lambda^2 - 2\lambda B} - \gamma\,N. \tag{7}$$

These Schlapp expressions contain no distortion terms. By comparing Mizushima's expressions with the Schlapp formula, the distortion terms can be easily inserted without going back to the original rotational Hamiltonian.

The energy levels are schematically shown in Figure 101(b) of Herzberg's textbook. Each N level splits into three levels except for N = 0. An

extensive study has been conducted on the $^{16}O_2$ molecule because of obvious atmospheric interest. Both homonuclear $^{16}O_2$ and $^{18}O_2$ have only the rotational level of odd N values, because of restriction placed by the nuclear spin statistics. The NH molecule being heteronuclear is free from this restriction. The rotational levels of all N values, both even and odd, are allowed. The lowest rotational level of $J = 1$, $N = 0$, is perturbed by an offset of $-\frac{2}{3}\lambda + \gamma$ with respect to the non-perturbed, non-existing level of $J = 0$, $N = 0$.

In the NH spectrum shown in Figure 6 of Section I, strong lines form a structure closely resembling the P and R branch of the $^1\Sigma$ system. A close inspection reveals that the transitions involving $N = 1$ and $N = 0$ are, indeed, a well-defined triplet structure. We find that the major transitions of $\Delta N = \Delta J = \pm 1$ (i.e., $N+1_{N+2} - N_{N+1}$, $N+1_{N+1} - N_N$, and $N+1_N - N_{N-1}$) form a well-defined group for low N and that they become unresolvable as N gets larger. (We use the notation N_J for designating a level specified by $N = N$ and $J = J$.) The satellite transitions for $\Delta N = \pm 1$, and $\Delta J = 0$ (i.e., $N+1_{N+1} - N_{N+1}$, $N+1_N - N_N$, and so forth) are observable for low N, and those for $\Delta N = \pm 1$ and $\Delta J = \mp 1$ are found very weak.

The observed line positions given in Table I were used for the spectral analysis. Their designation is conformed with that used for the $^1\Sigma$ system, because a majority of strong lines formed by a blended mixture of the major transition, $\Delta N = \Delta J = \pm 1$, are structured very similar to the $^1\Sigma$ system. The line designated by P(N) is actually composed of a major-transition triplet, $(N-1_{N-2} - N_{N-1})$, $(N-1_N - N_{N+1})$, and $(N-1_{N-1} - N_N)$, and that by R(N) is a triplet, $(N+1_N - N_{N-1})$, $(N+1_{N+1} - N_N)$, and $(N+1_{N+2} - N_{N+1})$. The calculated

positions were obtained by the revised Schlapp formula which includes the distortion term. For the lines not fully resolved into a triplet structure, they were determined by counting all transitions in a close vicinity with a proper strength factor. The transitions which occur between N = 0 and N = 1 are split into a well-defined triplet structure. The position given for R(0) is for the position of 0_1-1_1 and P(1) for 1_1-0_1. The spectroscopic constants listed in Table II were determined using all observed line positions. In so doing, we came across a puzzling fact that the rotational parameters B, α, D etc. thus determined a good fitting to the observed line positions within a given vibrational transition (r.m.s. error $\sim$ 0.01 cm^{-1}), while the vibrational parameters ω_e, $\omega_e x_e$, and $\omega_e y_e$ failed to produce a good fitting on the vibrational center frequencies (r.m.s. error $\sim$ 0.1 cm^{-1}). No conclusions have been reached on the origin of error found on the vibrational fitting. Malicet et al[11] reported the band center $\Delta G_{1/2}$ and $\Delta G_{3/2}$ of the $^3\Sigma$ state as 3125.49 cm^{-1} and 2968.89 cm^{-1}. Their values for ω_e and $\omega_e x_e$ are 3282.09 cm^{-1} and 78.3 cm^{-1}, respectively. [The value of ω_e quoted in their original paper contains an obvious arithmetic error.] Our observed values for the band center are $\Delta G_{1/2}$ = 3125.589, $\Delta G_{3/2}$ = 2969.518, $\Delta G_{5/2}$ = 2812.604, and $\Delta G_{7/2}$ = 2654.848. Our values for ω_e = 3280.85 cm^{-1}, $\omega_e x_e$ = 77.40 cm^{-1}, and $\omega_e y_e$ = -.14 cm^{-1} have a better accuracy than those determined using the uv data.

References

1. P. Hansen and H. Sakai, AFGL-TR-79-0150 (1979).
2. G. Herzberg, Molecular Spectra & Molecular Structure, I. Spectra of Diatomic Molecules, D. van Nostrand (1950).
3. H.A. Kramers, Zeits. f. Physik 53, 422 (1929).

4. M.H. Hebb, Phys. Rev. 49, 610 (1936).

5. R. Schlapp, Phys. Rev. 51, 342 (1937).

6. S.L. Miller and G.H. Townes, Phys. Rev. 90, 537 (1953).

7. M. Mizushima and R.N. Hill, Phys. Rev. 93, 745 (1954).

8. B.G. West and M. Mizushima, Phys. Rev. 143, 31 (1966).

9. W. Steinbach and W. Gordy, Phys. Rev. A, 8, 1753 (1973).

10. M. Mizushima, The Theory of Rotating Diatomic Molecules, Wiley & Sons (1975).

11. J. Malicet et al, J. Chim. Phys. Fr. 67, 25 (1970).

Table I

Observed line position of the NH infrared band

N	R branch observed position cm^{-1}	o-c cm^{-1}	wt	P branch observed position cm^{-1}	o-c cm^{-1}	wt
1-0 band						
0	3157.740*	-.032	1.0			
1	3187.050	-.013	1.0	3092.310*	.008	1.0
2	3215.740	.034	1.0	3059.090	-.003	1.0
3	3243.010	.009	1.0	3023.830	.025	1.0
4	3268.810	.005	1.0	2987.510	.012	1.0
5	3293.150	-.025	1.0	2950.080	-.015	1.0
6	3315.910	.008	.7	2911.580	-.043	.5
7	3337.150	.013	.4	2871.950	.038	.4
8	3356.840	-.008	.2	2831.480	.007	.1
2-1 band						
0	3007.070*	-.001	1.0			
1	3028.140	-.008	1.0	2937.310*	-.011	1.0
2	3055.580	.025	1.0	2905.390	-.003	1.0
3	3081.590	.008	1.0	2871.490	-.002	1.0
4	3106.150	-.007	1.0	2836.480	.007	1.0
5	3129.210	-.015	1.0	2800.350	.001	1.0
6	3150.710	-.001	.5	2763.110	.008	.7
7	3170.610	.030	.2	2724.840	-.014	.4
8	3188.800	.143	.0	2685.500	.008	.0

*see the text

N	R branch observed position cm^{-1}	o-c cm^{-1}	wt	P branch observed position cm^{-1}	o-c cm^{-1}	wt
3-2 band						
0	2842.220*	.005	.7			
1	2868.990	-.014	.8	2782.080*	.009	.8
2	2895.090	.021	1.0	2751.440	.005	1.0
3	2919.770	-.006	1.0	2718.840	-.029	1.0
4	2942.980	-.008	1.0	2685.050	.009	.9
5	2964.700	-.004	.8	2650.160	-.002	.8
6	2984.890	.010	.5	2614.100	.052	.4
7	3003.550	-.001	.1	2577.120	-.038	.3
8	3020.590	.021	.0	2538.840	.149	.0
4-3 band						
0	2682.830*	.072	.5			
1	2708.370	.017	1.0	2625.390*	-.038	1.0
2	2733.140	.015	1.0	2595.950	-.003	1.0
3	2756.480	.019	1.0	2564.520	.033	1.0
4	2778.310	.044	1.0	2532.060	-.027	.5
5	2798.680	.005	.3	2498.430	.062	0.0
6	-			2463.710	.096	0.0
7	2834.840	.045	.0	-		
8				-		

*see the text

Table II

Spectroscopic constants of NH electronic ground state ($X^3\Sigma$)

ω_e	3280.85 cm^{-1}
$\omega_e x_e$	77.40 cm^{-1}
$\omega_e y_e$	-.14 cm^{-1}
B_e	16.674 cm^{-1}
α_e	.650 cm^{-1}
D_e	17.6 x 10^{-4} cm^{-1}
β	-.41 x 10^{-4} cm^{-1}
λ_0 *	.911 cm^{-1}
λ_1 *	-.013 cm^{-1}
γ_0 †	-.055 cm^{-1}
γ_1 †	.0037 cm^{-1}

* $\lambda = \lambda_0 + \lambda_1 \nu$

† $\gamma = \gamma_0 + \gamma_1 \nu$

III. Excitation of N_2 and Formation of NH

The following brief analysis is presented to develop an understanding (1) of the role played by the nitrogen molecules in the infrared radiative processes, and (2) of the formation mechanism of NH observed in our glow discharge source.

The electronic energy states of N_2 listed in Table I are classified into two major categories, the triplets and the singlets.[1] The adiabatic molecular potentials of the triplet state are shown in Fig. 1, and those of the singlet in Fig. 4. The glow discharge excites these levels by means of the electronic collision. The integral cross-sections for the electronic excitation have been experimentally determined by Cartwright et al as a function of the incident electron energy.[2,3] They are shown in Fig. 2 for the triplets, and in Fig. 5 for the singlets. The excitation to the $C^3\pi_u$ state seems most efficient compared with other excitations in an energy range below 20 ev. The de-excitation by means of interaction to the radiative field is specified by the transition probability, shown in Fig. 3 for the triplets and in Fig. 6 for the singlets. The singlet states de-excite to the ground state at a rate much faster than the triplet states.[4] The radiative transitions observable in the infrared region are:

(1) the first positive band of $B^3\pi_g - A^3\Sigma_u^+$

(2) the Wu-Benesch band of $W^3\Delta_u - B^3\pi_g$

(3) the McFarlane IR band of $w^1\Delta_u - a^1\pi_g$

(4) the McFarlane IR band of $a^1\pi_g - a'^1\Sigma_u^-$.

In our glow discharge excitation, all states shown in Figures 1 and 4 would be produced as a result of the direct excitation by the electronic

collision. The energy available in the glow discharge for the excitation is certainly high enough for the transitions. The produced atomic oxygen emission furnished supporting data for the excitation.[5] The upper state $B^3\pi_g$ for the first positive band transition is populated by three possible mechanisms:

(1) the direct excitation by means of the electronic collision;

(2) the intersystem cascading from the $W^3\Delta_u$;

(3) the intersystem cascading from the $C^3\pi_u$.

The Wu-Benesch band transition involves radiative transfer to and from $W^3\Delta_u$ which is populated by both the direct excitation from the ground state and the intersystem cascade. The transition is inter-related to the first positive band, since it is one of the populating mechanisms to the B state. Both transitions of the McFarlane IR bands are interconnected; the $w^1\Delta_u$ is populated by the direct excitation, and the $a^1\pi_g$ is populated by both the direct and the intersystem cascading process w→a. There should be a definite distinction in the infrared emission of N_2 between that produced by the triplet system and by the singlet system. The former is always accompanied by the first positive band observable in the near infrared, and the latter is devoid of it. When the incident electron energy is above 30 ev, the emission by the singlet system would dominate because of a large cross-section for the $a^1\pi_g$ state in the region. In contrast to this situation, when the electron energy is below 30 ev, the emission by the triplet system would take over. The glow discharge condition obtained in our experimental setup favors the emission by the triplet system, dictated by the average electronic acceleration between the collisions.

The $C^3\pi_u$ state, having a rather large cross-section in the lower

electron energy range, may play an interesting role in the excitation mechanism of our glow discharge source. The state is characterized by the decomposition to $N(^4S^0) + N(^2D^0)$ with a low dissociation energy of $\sim$ 1 ev. If in the glow discharge a product is formed in a reaction of N_2 with an atom, say X, specified by $N_2^* + X \rightarrow NX + N$, the $C^3\pi_u$ state is able to serve as a very plausible candidate for the reaction because of its low dissociation energy. The proposed process above is a good candidate for a recombination mechanism of the observed NH infrared band. The adiabatic molecular potentials of NH sketched in Fig. 7 show that the $A^3\pi_i$ state of NH decomposes to $N(^2D^0) + H(^2S)$, and it has a dissociation energy estimated 2.6 ev. The atomic hydrogen is certainly abundant in our glow discharge source,[5] evidenced by many observable infrared HI lines. It is a safe assumption that the atomic hydrogens are available as a reactive collision partner. Thus it is very possible that an exothermic reaction

$$N_2\ (C^3\pi_u) + H(^2S) \rightarrow NH\ (A^3\pi_i) + N(^4S^0)$$

would occur in our discharge source. The ground state $X^3\Sigma^-$ of NH is formed by de-exciting the $A^3\pi_i$ state. The $C^3\pi_u$ state of N_2 de-excites to the $B^3\pi$ state rather quickly with a lifetime $\sim 5 \times 10^{-8}$ sec. The exchange reaction above is required to occur at a rate faster than this value.

References

1. A. Lofthus and P. Krupenie, J. Phys. Chem. Ref. Data 6, 113 (1977).
2. D.C. Cartwright et al, Phys. Rev. A 16, 1013 (1977).
   D.C. Cartwright et al, Phys. Rev. A 16, 1041 (1977).
   A. Chatjian et al, Phys. Rev. A 16, 1052 (1977).
3. N.F. Lange, Rev. Mod. Phys. 52, 29 (1980).
4. D.C. Cartwright, J. Geophysical Res. 83, 517 (1978).
5. P. Hansen and H. Sakai, AFGL-TR-79-0150 (1979).

Table I

State	T_e	N.O. Configuration $(1\sigma_u)(2\sigma_g)(1\pi_g)(3\sigma_u)$ other	Diss. Products N + N	Dissociation Energy D_e^0	ω_e	$\omega_e x_e$	$\omega_e y_e$	Observed transition	System name	Spectral region (Å)	References
$4'(^1\Sigma_u^-$ or $^1\Delta_u)$	111333							5'-a?			210
$e_3\ ^1\Pi_u$	105710.4	3 2 Ry $n\sigma_g$			1987.4	16.3		e_3-X		950-880	675,414
$H^3\Phi_u$	(105,000)	3 1 2 0	$^2D^o+^2D^o$	(12163)	924.21	12.29	-0.173	H-G	Gaydon-Herman green	6370-5040	131
$c_4'\ ^1\Sigma_u^+$	104323.3	4 1 0 0 Ry $n\rho\pi_u$			2201.78	25.199	0.7874	c_4'-X	Carroll-Yoshino Ry series	960-805	132,414
$c_3\ ^1\Pi_u$	104138.2	4 1 Ry $n\rho\pi_u$			2192.20	14.70		c_n-a" c_3^n-X	Lesbetter Ry series Worley-Jenkins Rydberg series	865-820 960-780	408 130,414, K. Yoshino, (Private communication)
$b'\ ^1\Sigma_u^+$	103670.8	4 1	$^2D^o+^2P^o$	23806	760.98	4.418	0.1093	b'-X		1290-820	132,414,660
$D^3\Sigma_u^+$	(103573)	4 1 Ry $n\rho\sigma_u$						D-B		2900-2250	257
$b^1\Pi_u$	100817.5		$^2D^o+^2D^o$	16345				(b',c,c',e,d'-a) b-a b-X	Gaydon-Herman singlet	3670-2220 1110-850	130,414
$a''^1\Sigma_g^+$	98840.30	4 1 0 0 Ry $3s\sigma_g$						a"-X	Tresslar-Lutz	1010	408
$C'^1\Pi_u$	97603.56	3 1 2 0	$^4S^o+^2D^o$	(334)				C'-E	Goldstein-Kaplan	5080-2860	128
$E^1\Sigma_g^+$	(95774.50)	4 1 0 0 Ry $3s\sigma_g$	$^4S^o+^2D^o$	2163	[2185]			E-A	Herman-Kaplan	2740-2130	133
$^5\Pi_u$	(93200)	3 1 2 0	$^4S^o+^2D^o$								136
$C^1\Pi_u$	88977.84	4 2 1 $-2\sigma_u$	$^4S^o+^2D^o$	8960	2047.178	28.4450	2.08833	C-B C-X	2+ Tanaka	5460-2680 1130-1070	196,175 612
$G^3\Delta_g$	(87100)	2 2 2	$^4S^o+^2D^o$	(10800)	765.9	11.85					131
$^3\Sigma_g^+$	(77900)	(2 2 2 0 / 3 1 1 1)	$^4S^o+^4S^o$	(814)	(650)						126
$w^1\Delta_u$	72698.490	3 2 1 0	$^2D^o+^2D^o$	45465	1559.496	12.0078	0.04542	w-a w-X	McFarlane IR Tanaka	85000-35000 1400-1140	448-9 425
$a^1\Pi_g$	68951.210	4 1 1 0	$^2D^o+^2D^o$	48212	1694.1895	13.9430	0.007864	a-a' a-X	McFarlane IR Lyman-Birge-Hopfield	85000-39000 2600-1100	448 462-4,627-8
$a'^1\Sigma_u^-$	67739.290	3 2 1 0	$^2D^o+^2D^o$	49424	1530.2675	12.0778	0.041534	a'-X	Ogawa-Tanaka-Wilkinson-Mulliken	2000-1080	615,449
$B'^1\Sigma_u^-$	65852.35	3 2 1 0	$^4S^o+^2P^o$	41701	1516.883	12.1811	.041864	B'-B B'-X	IR afterglow Ogawa-Tanaka-Wilkinson	8900-6050 2240-1120	138 611
$W^3\Delta_u$	59380	3 2 1 0	$^4S^o+^2D^o$	38558	1501.4	11.6		W-B	Wu-Benesch	43000-22000	67
$B^3\Pi_g$	59306.81	4 1 1 0	$^4S^o+^2D^o$	38631	1733.391	14.1221	-0.05688	B-A B-Y	1+ Wilkinson	25310-4780 1685-1640	196
$A^3\Sigma_u^+$	49754.78	3 2 1 0	$^4S^o+^4S^o$	28959	1460.638	13.8723	-0.01030	A-X	Vegard-Kaplan	5325-1250	196,462
$X^1\Sigma_g^+$	0	4 2 0 0	$^4S^o+^4S^o$	78714	2358.5685	14.3144	-0.002258				421,462,464,627,111

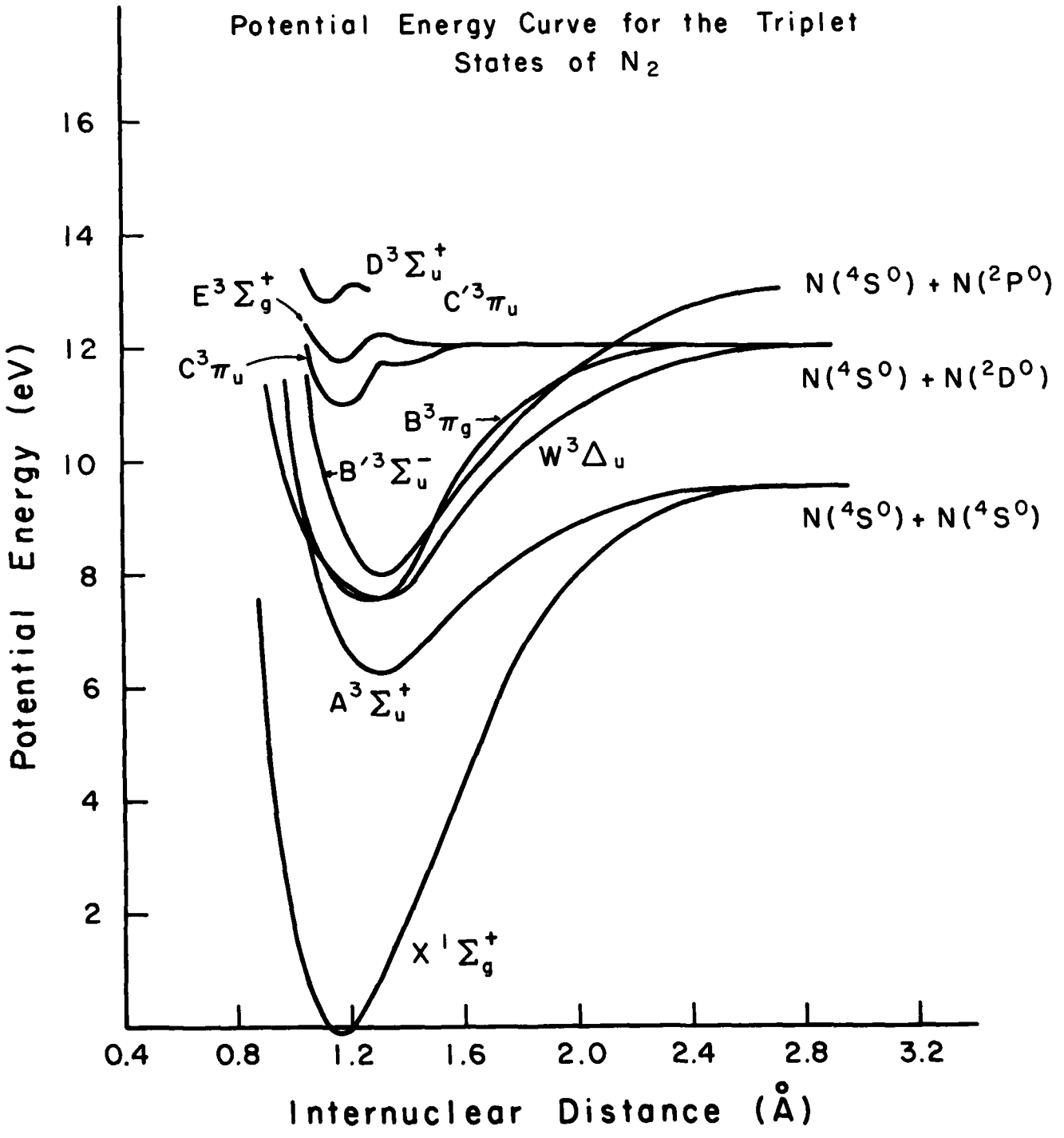
Potential Energy Curve for the Triplet States of N_2
Potential Energy (eV)
16
14
12
10
8
6
4
2
0.4
0.8
1.2
1.6
2.0
2.4
2.8
3.2
Internuclear Distance (Å)
$D^3\Sigma_u^+$
$E^3\Sigma_g^+$
$C'^3\pi_u$
$C^3\pi_u$
$B^3\pi_g$
$B'^3\Sigma_u^-$
$W^3\Delta_u$
$A^3\Sigma_u^+$
$X^1\Sigma_g^+$
$N(^4S^0) + N(^2P^0)$
$N(^4S^0) + N(^2D^0)$
$N(^4S^0) + N(^4S^0)$

FIGURE 1

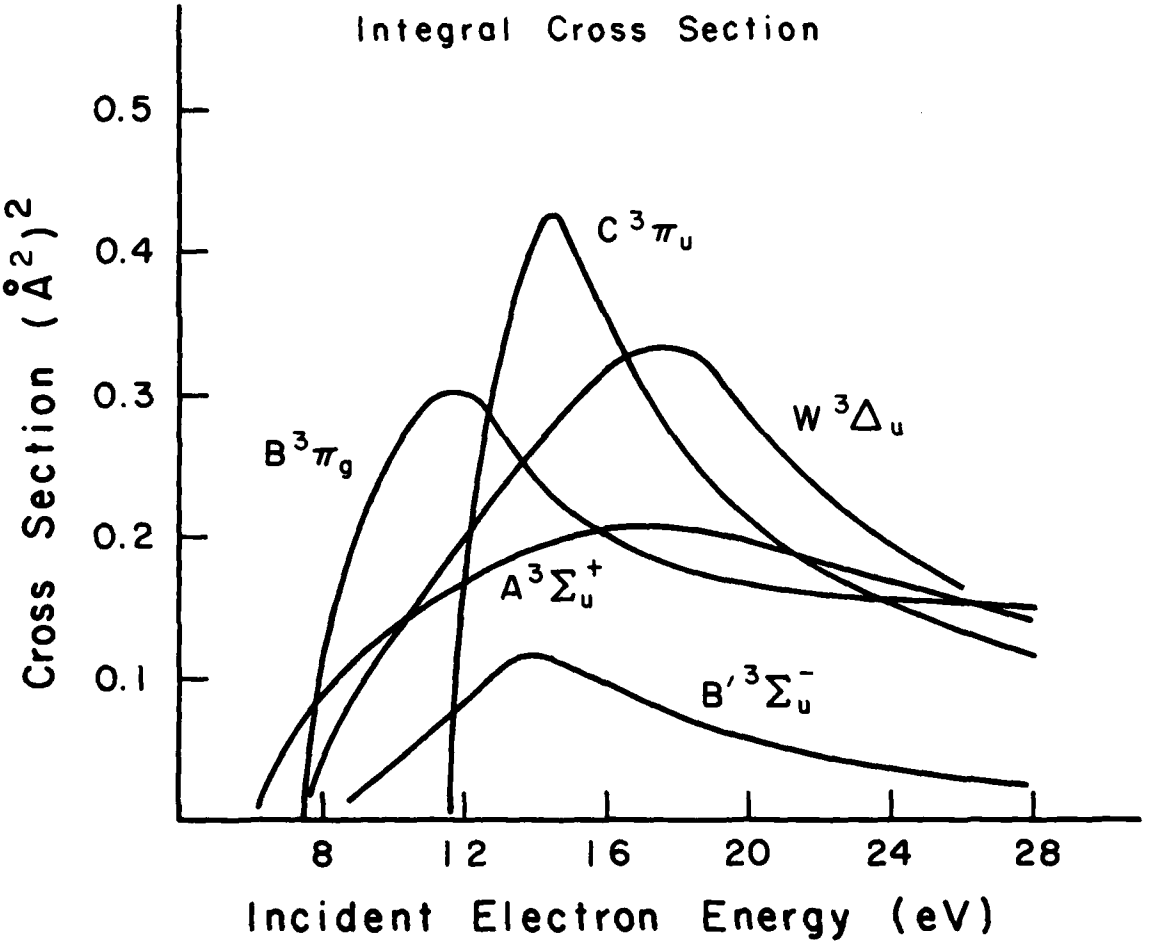
Integral Cross Section
Cross Section ($Å^2$)
0.5
0.4
0.3
0.2
0.1
$C\,^3\pi_u$
$W\,^3\Delta_u$
$B\,^3\pi_g$
$A\,^3\Sigma_u^+$
$B'\,^3\Sigma_u^-$
8
12
16
20
24
28
Incident Electron Energy (eV)

FIGURE 2

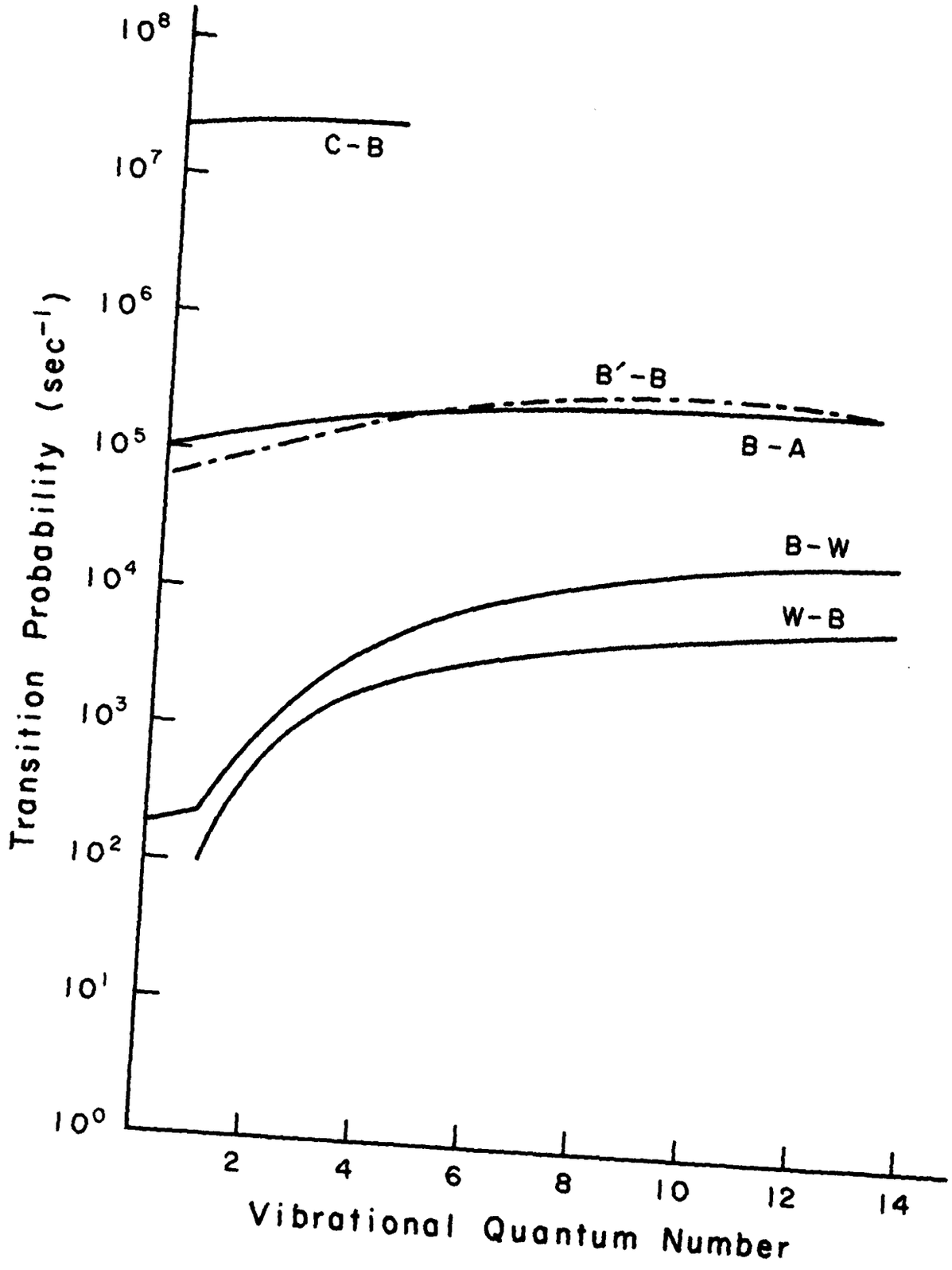
10^8
10^7
10^6
10^5
10^4
10^3
10^2
10^1
10^0
Transition Probability (sec^{-1})
C-B
B′-B
B-A
B-W
W-B
2
4
6
8
10
12
14
Vibrational Quantum Number

FIGURE 3

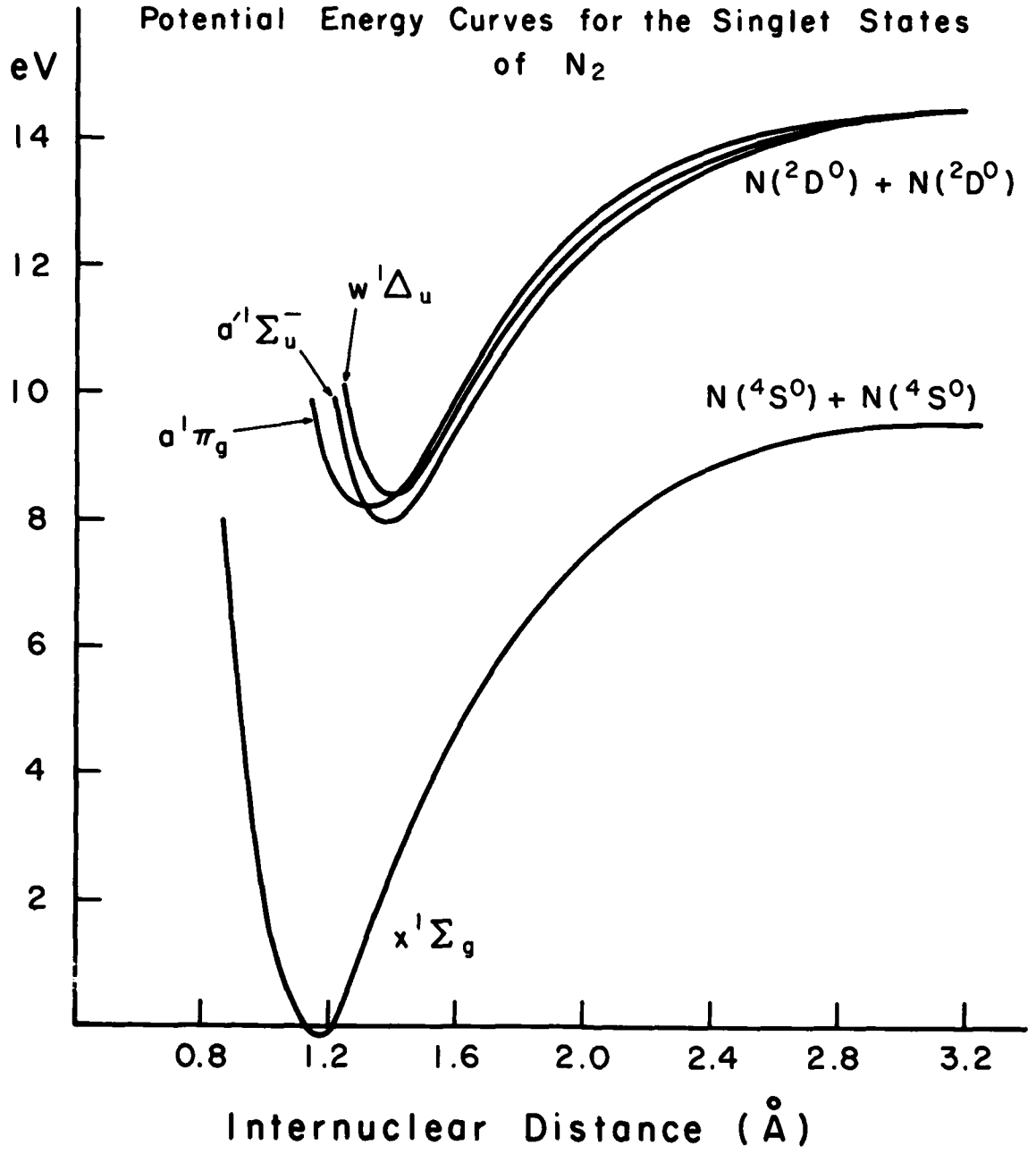
Potential Energy Curves for the Singlet States of N_2
eV
14
12
10
8
6
4
2
$N(^2D^0) + N(^2D^0)$
$w\,^1\Delta_u$
$a'\,^1\Sigma_u^-$
$a\,^1\pi_g$
$N(^4S^0) + N(^4S^0)$
$x\,^1\Sigma_g$
0.8
1.2
1.6
2.0
2.4
2.8
3.2
Internuclear Distance (Å)

FIGURE 4

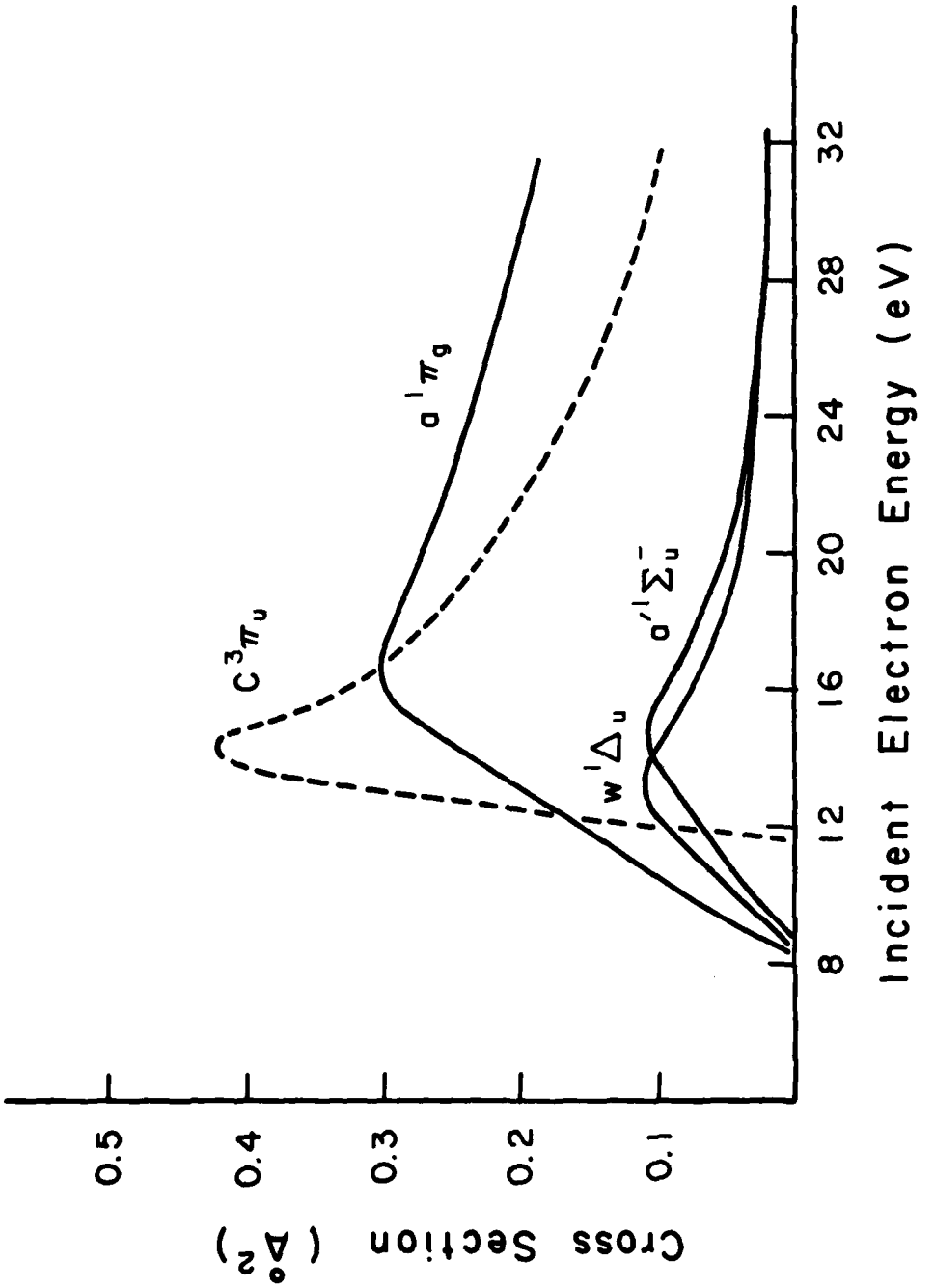
Cross Section (A^2_o)
0.5
0.4
0.3
0.2
0.1
8
12
16
20
24
28
32
Incident Electron Energy (eV)
$c^3\pi_u$
$a^1\pi_g$
$w^1\Delta_u$
$a'^1\Sigma_u^-$

FIGURE 5

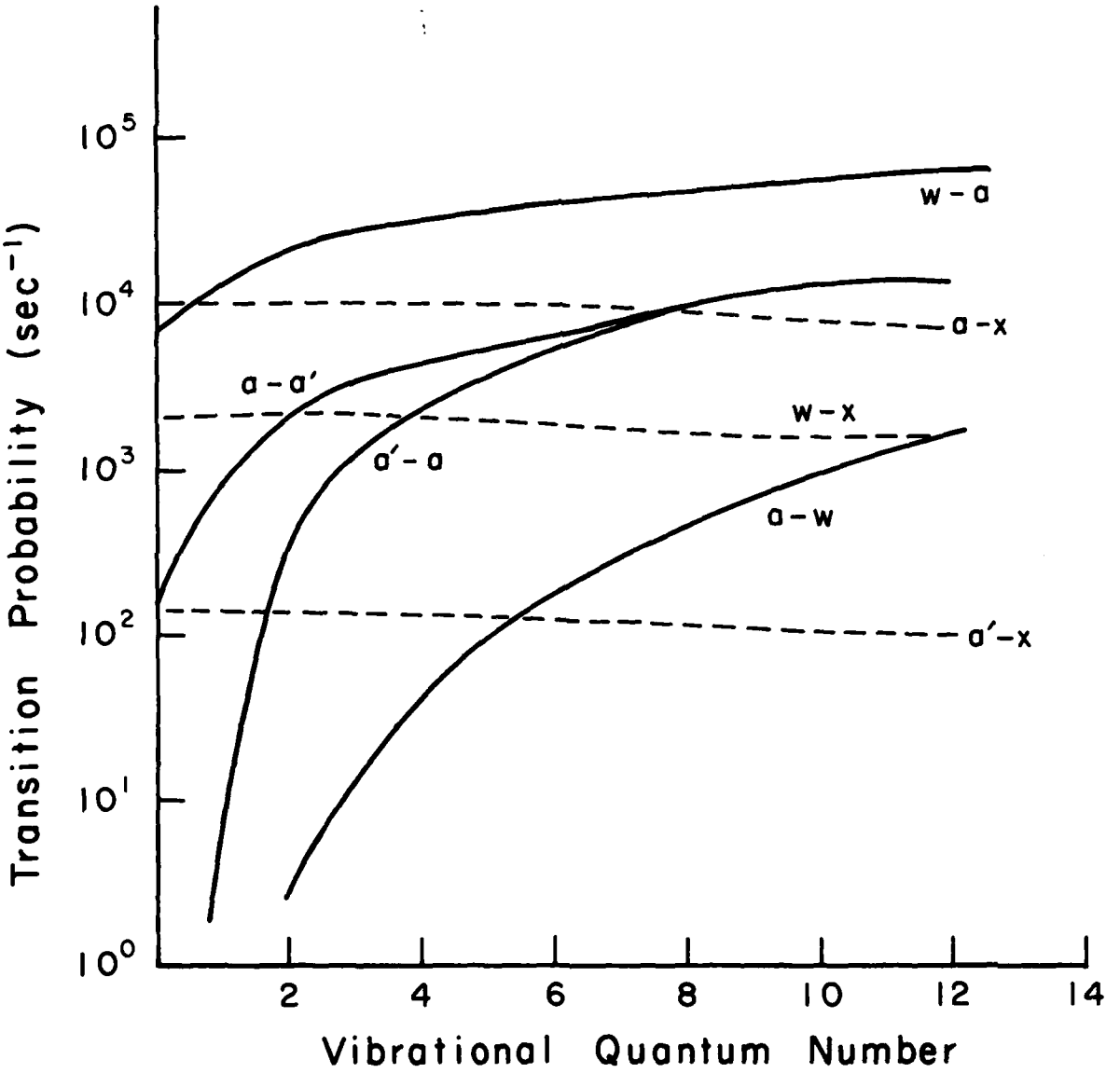
Transition Probability (sec⁻¹)
10⁵
10⁴
10³
10²
10¹
10⁰
2
4
6
8
10
12
14
Vibrational Quantum Number
w - a
a - x
a - a'
w - x
a' - a
a - w
a' - x

FIGURE 6

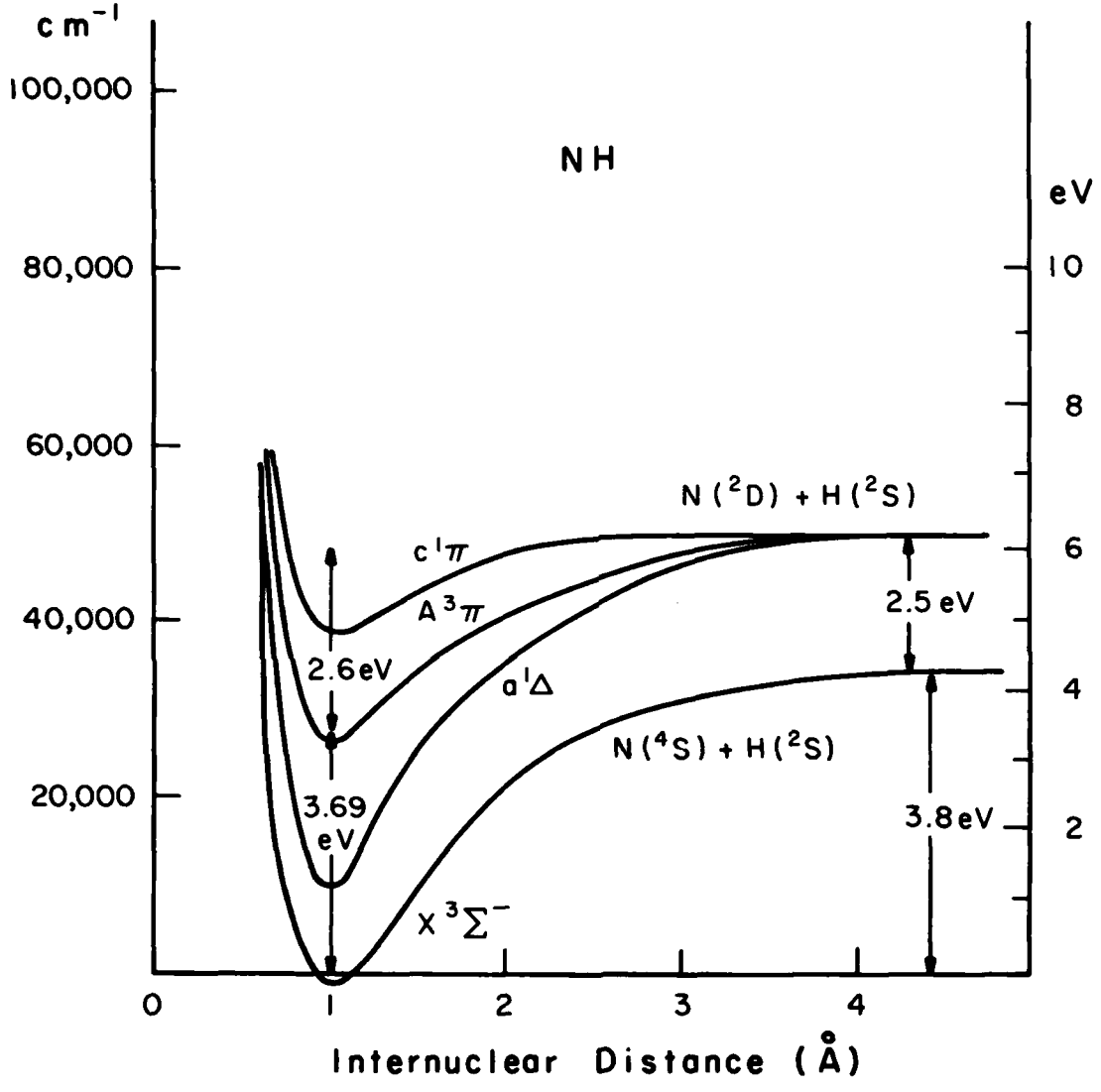
cm⁻¹
100,000
80,000
60,000
40,000
20,000
NH
eV
10
8
6
4
2
N(²D) + H(²S)
c¹π
A³π
a¹Δ
2.5 eV
2.6eV
N(⁴S) + H(²S)
3.69 eV
3.8eV
X³Σ⁻
0
1
2
3
4
Internuclear Distance (Å)

FIGURE 7


ATE
LME